JOURNAL OF BACTERIOLOGY, Nov. 2007, p. 8005–8014 Vol. 189, No. 22
0021-9193/07/$08.00+0 doi:10.1128/JB.00566-07

Motility and Chemotaxis in *Agrobacterium tumefaciens* Surface Attachment and Biofilm Formation▽†

Peter M. Merritt, Thomas Danhorn, and Clay Fuqua*

Department of Biology, Indiana University, Bloomington, Indiana 47405

Received 12 April 2007/Accepted 24 August 2007

Bacterial motility mechanisms, including swimming, swarming, and twitching, are known to have important roles in biofilm formation, including colonization and the subsequent expansion into mature structured surface communities. Directed motility requires chemotaxis functions that are conserved among many bacterial species. The biofilm-forming plant pathogen *Agrobacterium tumefaciens* drives swimming motility by utilizing a small group of flagella localized to a single pole or the subpolar region of the cell. There is no evidence for twitching or swarming motility in *A. tumefaciens*. Site-specific deletion mutations that resulted in either aflagellate, flagellated but nonmotile, or flagellated but nonchemotactic *A. tumefaciens* derivatives were examined for biofilm formation under static and flowing conditions. Nonmotile mutants were significantly deficient in biofilm formation under static conditions. Under flowing conditions, however, the aflagellate mutant rapidly formed aberrantly dense, tall biofilms. In contrast, a nonmotile mutant with unpowered flagella was clearly debilitated for biofilm formation relative to the wild type. A nontumbling chemotaxis mutant was only weakly affected with regard to biofilm formation under nonflowing conditions but was notably compromised in flow, generating less adherent biomass than the wild type, with a more dispersed cellular arrangement. Extragenic suppressor mutants of the chemotaxis-impaired, straight-swimming phenotype were readily isolated from motility agar plates. These mutants regained tumbling at a frequency similar to that of the wild type. Despite this phenotype, biofilm formation by the suppressor mutants in static cultures was significantly deficient. Under flowing conditions, a representative suppressor mutant manifested a phenotype similar to yet distinct from that of its nonchemotactic parent.

The ability of bacteria to propel themselves through their environment, often in response to chemical and physical gradients, is an important adaptive mechanism that promotes optimal positioning of cells at microscopic spatial scales. Generally, motile bacteria move through fluids and along surfaces by using external appendages, including pili and flagella. Rotation of single or multiple flagella drives swimming motility in fluid environments and swarming along wetted surfaces (4). *Escherichia coli*, with the best-understood model system of bacterial motility, moves unidirectionally, with periodic pauses that involve active tumbling, which reorient the cell prior to continued forward motion (4). This essentially random movement can be biased through taxis mechanisms that modify the frequency of reorientation. Motility by other species, including members of the *Alphaproteobacteria*, can differ significantly from the *E. coli* paradigm, although other species often employ conserved mechanisms (40). Type IV pili also mediate cellular movement along surfaces, in a process called twitching motility, by directional extension and subsequent depolymerization of the pili (25). Other microbes utilize gliding and ratchet-like mechanisms to move on surfaces (27).

Motility can have a profound impact on the colonization of surfaces, the first step in the formation of adherent microbial assemblies called biofilms. Subsequent accumulation and lateral expansion of adherent biomass can also involve motility. It has been shown that aflagellate (Fla$^-$) *E. coli* mutants do not attach to surfaces in static culture (33). Active motility is required for adherence, as nonmotile *E. coli* mutants that make flagella but cannot rotate them (Mot$^-$) are also deficient in biofilm formation (33). Mutations that disrupt flagellar biosynthesis and twitching motility significantly alter biofilm formation and architecture in several pseudomonads (21, 32). *Serratia marcescens* requires swarming motility via flagella and surfactant production to effectively colonize surfaces (23). The ability to rapidly spread across surfaces after initial attachment, which is dependent on both flagella and pili, provides *Pseudomonas aeruginosa* with a significant competitive advantage in mixed-species biofilms (2). Less direct evidence exists for the impact of chemotaxis on surface interactions. Mutations that disrupt the chemotaxis sensor kinase *cheA*, resulting in nontumbling mutants, do not affect biofilm formation by *E. coli*. Similar chemotaxis mutants of *Aeromonas* spp. are reported to manifest severe biofilm defects (20, 33). Colonization of surfaces as a monolayer by *Vibrio cholerae* also involves chemotaxis (31). In these systems, the mechanistic basis for the chemotaxis requirement in biofilm formation remains unclear.

Agrobacterium tumefaciens is a member of the *Alphaproteobacteria* that forms complex biofilms on abiotic surfaces and plant tissues (10, 34). *A. tumefaciens* is best known as the causative agent of crown gall, a neoplastic disease of plants. Pathogenesis involves the horizontal transmission of a segment of *A. tumefaciens* DNA, carried on the tumor-inducing (Ti) plasmid, into the host plant genome (14). Genes on the transferred DNA direct a hormonal imbalance in the plant that

* Corresponding author. Mailing address: Department of Biology, Indiana University, 1001 E. 3rd St., Jordan Hall 142, Bloomington, IN 47405-1847. Phone: (812) 856-6005. Fax: (812) 855-6705. E-mail: cfuqua@indiana.edu.

† Supplemental material for this article may be found at http://jb.asm.org/.

▽ Published ahead of print on 31 August 2007.

results in uncontrolled proliferation of plant cells, forming the characteristic gall. Other transferred DNA genes direct the synthesis of specialized nutrients by the plant, which are consumed specifically by *A. tumefaciens* via catabolic pathways also encoded on the Ti plasmid. Intense efforts have been focused on the mechanics of this cross-kingdom genetic exchange, and the process has been harnessed effectively in plant transgenesis (8, 11, 14). However, our understanding of the activities that lead to plant association and productive attachment is far more limited. It is also important that many agrobacteria are present in the bulk soil as avirulent plant-associated commensals (5). Motility and chemotaxis have been implicated in plant association and the early steps of disease (6, 37), but a thorough analysis of their role in surface interactions has not been reported.

Swimming motility in the most commonly studied strain of *A. tumefaciens*, C58, is mediated by flagella, and there is no evidence of swarming or twitching motility (17). Multiple flagella are typically localized as a small tuft positioned at or around a single pole of the cell (6). Similar to the well-studied flagellar system of the related bacterium *Sinorhizobium meliloti*, the flagella are thought to rotate in a clockwise direction to propel the cell forward (3, 36). The current model states that tumbling is not caused by a reversal of flagellar rotation, as in the *E. coli* paradigm, but rather occurs through asynchronous slowing of flagellar rotation, resulting in chaotic motion of the flagella (3, 36). Flagellar assembly genes are carried in a single major cluster of genes on the *A. tumefaciens* C58 circular chromosome (Atu0542 to Atu0582), including four discrete flagellin gene homologues (15, 45). Mutants deleted for three of the four flagellin genes (Δ*flaABC*) are reported to be nonmotile and are attenuated for virulence (6). The genes for several motor (Mot) proteins, homologues of which drive flagellar rotation in other systems, are also located within this cluster, although these genes and their role in motility have not been studied thus far.

The *A. tumefaciens* C58 genome also encodes roughly 20 methyl-accepting chemotaxis protein (MCP) homologues, suggesting complex adaptive control over motility (15, 45). The main chemotaxis functions, including a single *cheA* gene encoding a two-component sensor kinase that interacts with the MCPs and two discrete response regulator genes (*cheY1* and *cheY2*), are located within the Che operon (Atu0514 to Atu0522), which is near the flagellar assembly cluster (46). This operon is syntenous to that found in *S. meliloti*, with the exception that *cheW* is not present (13). In contrast, there are two *cheW* homologues at separate positions on the C58 circular chromosome (Atu2075 and Atu2617). As in *S. meliloti*, there is no *cheZ* phosphatase gene homologue present in strain C58. A nonpolar *cheA* deletion mutant exhibited a smaller swim ring in motility agar and was less efficient than the wild type for tumorigenesis (46). Chemotaxis by *A. tumefaciens* towards phenolic plant exudates and opines has been demonstrated, and mutation of an MCP-type protein gene on the Ti plasmid abolished chemotaxis towards opines (19, 37).

In this study, we have generated and analyzed defined *A. tumefaciens* C58 mutants that are aflagellate (Δ*flgE*), flagellated but nonmotile (Δ*motA*), and motile but nonchemotactic (Δ*cheA*) for biofilm formation on abiotic surfaces in static culture and in flow cells. In so doing, we have also isolated an intriguing spontaneous suppressor of the chemotaxis mutation that reestablishes the ability to tumble but severely compromises biofilm formation. Our findings demonstrate important roles for chemotaxis and motility in biofilm formation under flowing and static conditions and show that biofilm attributes impacted by these functions can vary depending on prevailing environmental conditions.

TABLE 1. Strains and plasmids used in this study

Strain or plasmid	Relevant feature(s)	Source or reference
Strains		
A. tumefaciens strains		
C58	Nopaline type strain; pTiC58, pAtC58	42
PMM3	Δ*cheA* C58 derivative	This study
PMM4	Δ*flgE* C58 derivative	This study
PMM5	Δ*motA* C58 derivative	This study
cms-1 mutant	Spontaneous suppressor of PMM3	This study
E. coli strains		
SM10/λ*pir*	λ*pir* Tra^+; cloning strain	29
SY327/λ*pir*	λ*pir*; cloning strain	30
TOP10 F′	Cloning strain	Invitrogen
Plasmids		
pGEM-T Easy	PCR cloning vector; Ap^r	Promega
pBBR1MCS-2	Broad-host-range P_{lac} expression vector; Km^r	22
pKNG101	R6K ori; *sacB* (Suc^s) Sm^r	18
pJZ383	P_{tac}::*gfpmut3* Sp^r; pVS replicon	J. Zhu (9)
pPM104	pKNG101 carrying *cheA* SOE deletion fragment	This study
pPM107	pKNG101 carrying *flgE* SOE deletion fragment	This study
pPM108	pKNG101 carrying *motA* SOE deletion fragment	This study
pPM109	pBBR1MCS-2 P_{lac}::*cheA*	This study
pPM110	pBBR1MCS-2 P_{lac}::*flgE*	This study
pPM111	pBBR1MCS-2 P_{lac}::*motA*	This study

MATERIALS AND METHODS

Strains, plasmids, and growth conditions. All bacterial strains and plasmids used in this study are listed in Table 1. Reagents, antibiotics, and microbiological media were obtained from Fisher Scientific (Pittsburgh, PA) and Sigma-Aldrich (St. Louis, MO). DNA manipulations were performed following standard protocols (35), and DNA sequences were determined on an ABI 3730 sequencer (Indiana Molecular Biology Institute, Bloomington, IN). Oligonucleotide primers were supplied by Integrated DNA Technologies, Coralville, IA (primer information is listed in Table 2). Nucleic acid purification was performed using QIAquick Spin kits (QIAGEN, Valencia, CA). Plasmids were introduced into *A. tumefaciens* by electroporation (28) or conjugal transfer (12). Bacteria were maintained on either LB or AT minimal medium (39) supplemented with 0.5% (wt/vol) glucose and 15 mM ammonium sulfate (ATGN). To prevent the accumulation of iron oxide precipitate, the $FeSO_4 \cdot 7H_2O$ prescribed in the original AT recipe was omitted, with no adverse growth effect. For *sacB* counterselection, 0.5% sucrose (Suc) replaced glucose as the sole carbon source (ATSN). Antibiotic concentrations used were as follows: for *E. coli*, 100 μg ml^{-1} ampicillin, 25 μg ml^{-1} streptomycin (Sm), and 25 μg ml^{-1} kanamycin (Km); and for *A. tumefaciens*, 3 mg ml^{-1} Sm, 150 μg ml^{-1} Km, and 50 μg ml^{-1} spectinomycin, as required.

Construction of nonpolar markerless deletions. To generate nonpolar deletions, PCR was used to amplify approximately 500 bp of flanking sequence upstream (primers 1 and 2) and downstream (primers 3 and 4) of the reading frame to be deleted. Primers were designed to remove as much of the coding sequence as possible without disrupting any predicted translational coupling.

TABLE 2. Primer sequences

Primer	Sequence[a]
cheA 1	tctagaGCTGATGACGCTGAGAGGA
cheA 2	aagcttggtaccgaattcCGTGAAATGTCCCGTATC
cheA 3	gaattcggtaccaatcttAGGCGGATATCCAATGGC
cheA 4	ggatccTGATGAGACGCTTGACCTTG
cheA 5	CGGTGCTGGATCTCAACGA
cheA 6	GCCATTGCGTCATCAGGTT
cheA 7	ggtaccGTGAAACAGGAAACAGCTAATGGA TATGAACGAAATCA
cheA 8	tctagaATCCGCCTTCAACCCGTC
flgE 1	tctagaCTCGCTGGAAGCAACGCT
flgE 2	aagcttggtaccgaattcCATAGTGCCGAAAATACT CATT
flgE 3	gaattcggtaccaagcttCTGAAGAGATAATACTTC TCACGA
flgE 4	ggatccTGGGGCGATTGACGACA
flgE 5	CAGGGATCGCACGACGG
flgE 6	CGCCGTCAGTCGTGTAAAGC
flgE 7	ggtaccGTGAAACAGGAAACAGCTAATGAG TATTTTCGGCACTATG
flgE 8	tctagaCTCGTGAGAAGTATTATCTCTTCAG ATTG
motA 1	actagtTGCCGATGACACCTGATTTGG
motA 2	aagcttggtacctctagaGCAGCCGAAGGTGATTAT AAGT
motA 3	tctagaggtaccaagcttGTCGAGCAGGAGATGAT GAATC
motA 4	ggatccCGCTTTTTCCATTGGCAT
motA 5	TTGATTGTCGGTGCCTTGC
motA 6	GATGGTCACGCCGTAAAGG
motA 7	ggtaccGTGAAACAGGAAACAGCTAATGAA TATTGTAATTGGACTTAT
motA 8	tctagaTCATGCCGCCTTGTTTTC

[a] Engineered restriction sites are shown in lowercase. Underlining highlights the features engineered for optimized expression from the pBBR1-MCS2 vector (see Materials and Methods).

Primers 2 and 3 were designed with 18-bp complementary sequences at their 5′ ends (lowercase nucleotides in Table 2) to facilitate *s*plicing by *o*verlapping *e*xtension (SOE), essentially as described previously (41). Briefly, both flanking sequences were amplified using the high-fidelity Phusion DNA polymerase (NEB, Beverly, MA) and were agarose gel purified. Purified PCR products were used as both templates and primers for a five-cycle PCR. A final PCR step with primers 1 and 4, using 2 μl of the second-step reaction mix as the template, generated the full-length spliced product. The final PCR products were cloned into pGEM-T Easy (Promega, Madison, WI), confirmed by sequencing, excised by cleavage with the appropriate restriction enzyme, and ligated with the suicide vector pKNG101 cleaved at compatible restriction sites. The pKNG101 plasmid confers Sm resistance (Sm^r) and sucrose sensitivity (Suc^s) (18). Derivatives of pKNG101 were introduced into *A. tumefaciens* C58 by conjugal transfer. Because the R6K origin of pKNG101 does not replicate in *A. tumefaciens*, the plasmid must recombine into the genome to allow growth in media containing Sm. Recombinants were selected on ATGN plates containing Sm, and plasmid integration was confirmed by patching Sm^r isolates onto ATSN-Sm plates to identify Suc^s clones. To facilitate excision of the integrated plasmid, Sm^r Suc^s clones were grown overnight in ATGN broth without Sm and then plated on ATSN. Plasmid excision was verified by patching Suc^r clones onto ATSN plus Sm to identify Sm^s isolates. Appropriate deletion of the target genes was confirmed by diagnostic PCR and DNA sequencing of the products (with primers 5 and 6, which flank the target region).

Complementation constructs. To perform complementation analyses, wild-type coding sequences were cloned into pBBR1MCS-2 (22). 5′ primers were designed with a stop codon in frame with pBBR-carried *lacZ* followed by the *E. coli lacZ* ribosome binding site to prevent translational occlusion and to optimize expression, respectively (Table 2). Coding sequences for *cheA* (Atu0517), *flgE* (Atu0574), and *motA* (Atu0560) were PCR amplified from C58 genomic DNA, using the corresponding primers 7 and 8 for each gene (Table 2) and the Phusion polymerase, ligated into pGEM-T Easy, confirmed by sequencing, excised by restriction enzyme cleavage, and ligated with appropriately cleaved pBBR1MCS-2. Plasmid derivatives harboring the correct inserts were verified by restriction digestion and sequencing prior to electroporation into competent *A. tumefaciens* cells.

Flagellar staining and motility assays. A flagellar staining protocol was adapted from the work of Mayfield and Inniss (26). Briefly, a two-component stain [solution A is equal volumes 5% phenol and saturated $AlK(SO_4)_2 \cdot 12H_2O$ in 10% tannic acid, and solution B is 12% crystal violet (CV) in 100% ethanol] was mixed fresh at a ratio of 10 volumes solution A to 1 volume solution B, vortexed, and centrifuged to remove CV crystals. One microliter of cell culture was spotted onto a clean microscope slide and overlaid with a 22- by 22-mm coverslip. The slides were held vertically, and approximately 2 to 5 μl of stain was applied to the edge of the coverslip. Capillary action wicked the stain under the coverslip, staining the flagella. Samples were observed by phase-contrast microscopy using a 100× oil immersion objective after at least 5 min of staining.

Swimming and chemotaxis phenotypes were tested on ATGN swim agar plates containing 0.25% Bacto agar (BD, Sparks, MD) (1). Two plating formats were used. First, 100-mm petri plates were filled with 25 ml ATGN swim agar. Swim plates were inoculated from fresh colonies or cultures by using a toothpick that was stabbed into the agar at the center of the plate. Second, for screening purposes, 12-well tissue culture plates (Corning, Corning, NY) were filled with 3 ml swim agar per well and inoculated as described above.

Short-term binding assays. Short-term binding assays were conducted by growing the appropriate green fluorescent protein (GFP)-expressing strains in ATGN to an optical density at 600 nm (OD_{600}) of approximately 0.6. Glass coverslips were floated on 5 ml of culture in six-well tissue culture plates for 2 to 4 hours. Coverslips were removed from the plates, rinsed thoroughly with 1× AT buffer (79 mM KH_2PO_4, pH 7.0), and mounted on slides for microscopy. Each strain was tested in triplicate, with 10 fields of view captured for each coverslip by spinning disk confocal microscopy (Yokagawa CSU10 confocal scanner unit, Nikon TE2000U microscope, and Photometrics Cascade II 512B camera) with a 40× objective, using MetaMorph software (Molecular Devices Corp., Sunnyvale, CA). Cells were counted manually or automatically using ImageJ (NIH).

Cultivation and analysis of static culture biofilms. Static culture biofilms were grown essentially as described previously (34). Briefly, polyvinyl chloride (PVC) coverslips were placed vertically in 12-well polystyrene cell culture plates (Corning Inc.), inoculated with cells in ATGN at an OD_{600} of 0.05, and incubated at room temperature for 24 to 96 h. Biofilms were visualized macroscopically by CV staining or microscopically by phase-contrast and epifluorescence microscopy. For CV visualization, coverslips were rinsed in double-distilled H_2O, stained with 0.1% (wt/vol) CV, and rinsed again in double-distilled H_2O. Biomass adhered to the coverslip was quantified by soaking stained coverslips in 1 ml dimethyl sulfoxide (DMSO) to solubilize the CV and measuring the absorbance at 600 nm (A_{600}) in a Bio-Tek Synergy HT microplate reader. Absorbance values were normalized to culture growth by dividing the A_{600} value for solubilized CV by the OD_{600} of the planktonic cells.

Cultivation and analysis of flow cell biofilms. Once-through flow cells with a 200-μl chamber volume were inoculated with *A. tumefaciens* carrying pJZ383 (P_{tac}::*gfpmut3*) for GFP expression, as described previously (7, 10). All tubing and bubble traps were autoclaved prior to assembly of the flow cell system. The system was filled with 0.5% sodium hypochlorite and left overnight without flow. A minimum of 2 liters of sterile water was flushed through the system prior to treatment with 0.6% hydrogen peroxide at a flow rate of ~30 ml h^{-1} for at least 3 h. Flow cells were flushed with 2 to 3 liters of sterile water and then equilibrated with ATGN (flow rate of 3 ml h^{-1}) for at least 12 h prior to inoculation. For each strain tested, three individual flow channels were inoculated. Each chamber was inoculated with 200 μl of cells suspended in ATGN at an OD_{600} of 0.05. After 1 hour, flow was resumed at a rate of 3 ml h^{-1} and continued uninterrupted for the duration of the experiment. Five image stacks per channel were acquired on a spinning disk confocal microscope using MetaMorph software. Each field of view had an area of approximately 1.45×10^4 μm^2. Stacks were processed and analyzed using *auto*COMSTAT, a modified version of the COMSTAT biofilm evaluation package by Heydorn et al. (16; T. Danhorn and C. Fuqua, unpublished data). Biofilm parameters measured in this study were biovolume (μm^3 per μm^2 substatum area), substratum coverage (% within the first micrometer above the substratum), average height (μm), roughness (a unitless measure of height variability), and the total number of microcolonies counted in 15 fields of view.

RESULTS

Deletion mutations in motility and chemotaxis genes. To investigate the role of flagellar motility in biofilm formation, nonpolar, markerless deletions were generated in key genes encoding flagellar biosynthesis (Fla^-), flagellar rotation (Mot^-),

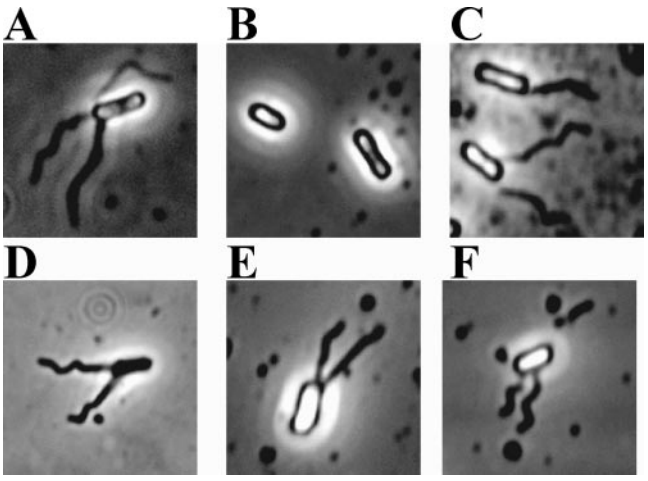

FIG. 1. Flagellar staining phenotypes of motility mutants. Phase-contrast images of CV-stained flagella from wild-type C58 and motility mutants are shown. Images were taken with a 100× objective. (A) C58 wild type; (B) Δ*flgE* mutant; (C) Δ*motA* mutant; (D) Δ*cheA* mutant; (E) Δ*flgE*/pPM110 mutant; (F) *cms-1* mutant.

and chemotaxis (Che$^-$) proteins. Precise deletions were generated in the *A. tumefaciens* C58 genes encoding the flagellar hook protein (*flgE*; Atu0574), a component of the flagellar motor (*motA*; Atu0560), and the chemotaxis sensor kinase (*cheA*; Atu0517). No motile Δ*flgE* or Δ*motA* cells were observed microscopically, while the Δ*cheA* mutant was motile but nontumbling (data not shown). Flagellar staining of the nonmotile mutants showed, as expected, that the Δ*flgE* mutant was aflagellate, while the Δ*motA* strain was flagellated (Fig. 1). Flagellar assembly and swimming were restored when wild-type copies of the deleted genes were expressed in *trans* (Fig. 1E and data not shown). All mutants grew at rates similar to that of the wild type in aerated cultures (data not shown).

Motility mutant swimming phenotypes were assessed on 0.25% swim agar plates. Neither the Δ*flgE* nor the Δ*motA* mutant expanded beyond the site of inoculation (Fig. 2B and C). Consistent with other *A. tumefaciens* Che$^-$ mutants (46),

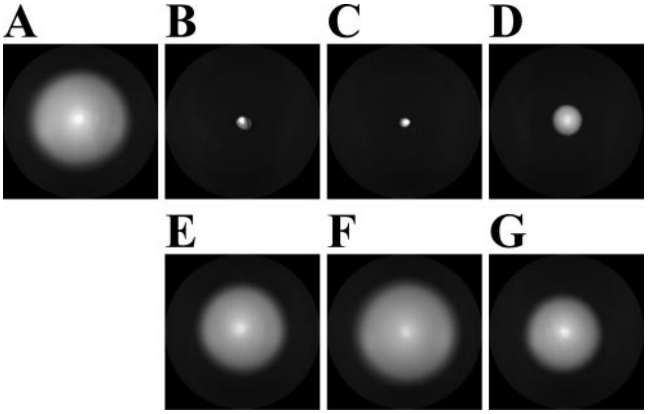

FIG. 2. Swim plate assays of C58 motility mutant and complemented mutant strains. ATGN plates supplemented with 0.25% agar were inoculated with wild-type C58 (A), the Δ*flgE* mutant (B), the Δ*motA* mutant (C), the Δ*cheA* mutant (D), the Δ*flgE*/pPM110 mutant (E), the Δ*motA*/pPM111 mutant (F), and the Δ*cheA*/pPM109 mutant (G).

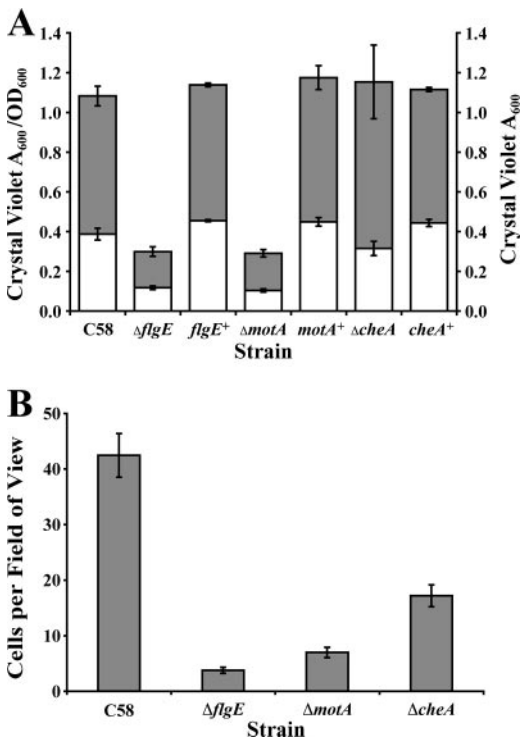

FIG. 3. Static biofilm formation and surface attachment by C58 motility mutants. (A) Quantification of DMSO-solubilized CV from PVC coverslip biofilms at 72 hpi. Biomass normalized for growth (A_{600}/OD_{600}; closed bars) and adherent biomass (CV A_{600}; open bars) are shown. +, strains carrying a wild-type copy of the deleted gene on pBBR1MCS-2 (Table 1). Error bars show standard errors of the means (SEM) for three coverslips. (B) Static culture short-term binding assay. Total numbers of attached cells per field of view (~3.13×10^4 μm^2) are shown. Values are averages of 30 fields of view. Error bars show SEM.

our Δ*cheA* mutant formed dense, small-diameter swim rings, in contrast to the diffuse, large-diameter swim rings observed in the wild type (Fig. 2D). For all of the mutants, normal swim phenotypes were restored by provision of a plasmid-borne copy of the deleted gene (Fig. 2E, F, and G).

Flagellar mutants are significantly compromised for attachment and biofilm formation. The C58 motility mutants were monitored for attachment and biofilm formation on PVC coverslips in ATGN. Under these conditions, the Δ*flgE* and Δ*motA* mutants were significantly deficient in their ability to form biofilms. The CV extracted from stained biofilms showed a >50% reduction of attached biomass for both mutants (Fig. 3A). Nonmotile mutants exhibited growth rates similar to that of the wild type in static cultures (data not shown). We conducted short-term binding assays to distinguish impaired attachment from deficiencies in subsequent biofilm maturation. In these assays, glass coverslips were floated on a dense suspension of cells for several hours and imaged by spinning disk confocal microscopy, and attached cells were counted. In these assays, the nonmotile mutants manifested a 90% reduction in attachment (Fig. 3B).

CV-stained Δ*flgE* biofilms on PVC coverslips manifested a macroscopic punctate pattern distinct from the pattern for wild-type biofilms (data not shown). Examination of coverslip biofilms grown with GFP-expressing Δ*flgE* mutants by epiflu-

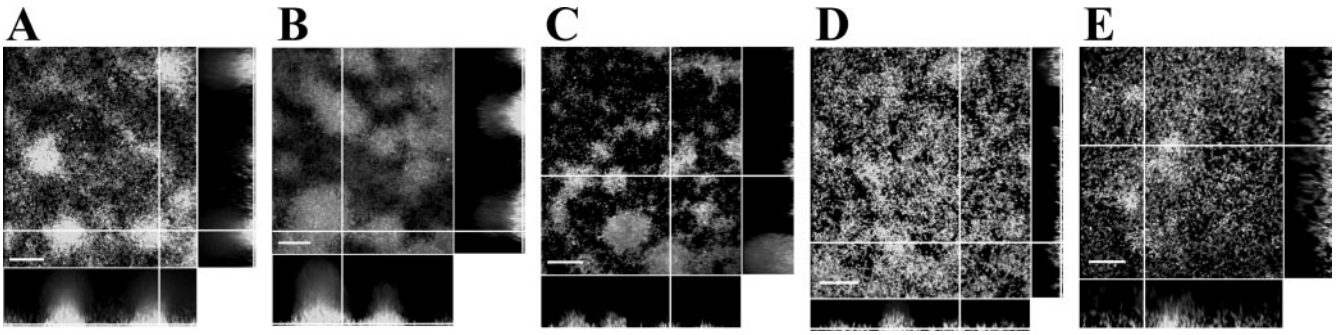

FIG. 4. Flow cell biofilms. Confocal laser scanning microscopy images of strain C58 and motility mutant derivatives expressing GFP grown in ATGN are shown. (A) C58 at 144 hpi; (B) Δ*flgE* mutant at 96 hpi; (C) Δ*motA* mutant at 144 hpi; (D) Δ*cheA* mutant at 144 hpi; (E) *cms-1* mutant at 144 hpi. Side and bottom panels are orthogonal views of the biofilms. Bar = 20 μm in all dimensions.

orescence microscopy revealed fewer attached cells but greater numbers of microcolonies than those in wild-type C58 biofilms (data not shown). The Δ*motA* mutant tended to manifest a more severe biofilm defect than the Δ*flgE* mutant, although this was not significant in all experiments (data not shown). Plasmid-borne copies of the deleted wild-type genes complemented each mutant biofilm phenotype.

Chemotaxis influences *A. tumefaciens* C58 attachment and biofilm formation in static culture. The Δ*cheA* mutant revealed a modest reduction in static culture biofilm formation relative to the wild type (Fig. 3A). However, when CV staining was normalized for culture growth (CV absorbance divided by planktonic culture turbidity), the relative amounts of adherent biomass were similar (Fig. 3A, gray bars). Static culture growth curves performed in the same format as the biofilm assays revealed a significant growth defect in the Δ*cheA* mutant that confounded interpretation of the Δ*cheA* biofilm phenotype (data not shown). Normal growth was restored by a plasmid-borne copy of wild-type *cheA*.

In order to assess surface interactions of the Δ*cheA* mutant independent of the growth rate, we conducted short-term binding assays as described above. At the time scale used in this experiment, the effects of growth were minimal. In this assay, the number of attached Δ*cheA* cells was approximately 40% of the wild-type cell number (Fig. 3B).

Robust biofilm formation in flow cells by Δ*flgE* mutants. We compared biofilm formation of the C58 motility mutants in once-through flow chambers under low-shear conditions. Flow cells are a continuous culture format in which the biofilm is constantly irrigated with fresh medium. In contrast to the marked biofilm deficiency observed in static assays, the Δ*flgE* mutant formed very thick and dense biofilms with numerous large towers by 96 h postinoculation (hpi) (Fig. 4B; see Fig. S1B in the supplemental material). After this point, the basic morphology of Δ*flgE* biofilms did not change. At 144 hpi, wild-type C58 biofilms were qualitatively similar to those of the Δ*flgE* mutant, indicating a significant acceleration in the rate of biofilm formation for the mutant but no gross alterations in biofilm architecture, aside from a pronounced difference in height (see Fig. S1A and B in the supplemental material).

We used a modified version of the COMSTAT biofilm analysis program (16), called *auto*COMSTAT (Danhorn and Fuqua, unpublished data), to quantitatively analyze flow cell biofilms. These analyses confirmed that the rate of Δ*flgE* biofilm formation was greatly accelerated relative to that of the wild type. By 96 hpi, biofilms formed by the Δ*flgE* mutant showed 5- to 15-fold increases in the total biovolume, percentage of substratum coverage, and average height relative to those of wild-type C58 (Fig. 5). The average maximum height from 15 fields of view was approximately 50 μm for Δ*flgE* biofilms at 120 hpi, in contrast to approximately 30 μm for the wild type at 144 hpi. The rate at which Δ*flgE* biofilms accumulated increased rapidly after 48 hpi, while a similar rate increase occurred only after 96 hpi in wild-type biofilms (Fig. 5). The maximum rates of biofilm formation were similar between the wild type and the Δ*flgE* mutant (compare Δ*flgE* mutant rates at 48 to 96 hpi to those of C58 at 96 to 144 hpi in Fig. 5). The Δ*flgE* mutant biofilms had saturated the flow cell system by 96 hpi, while

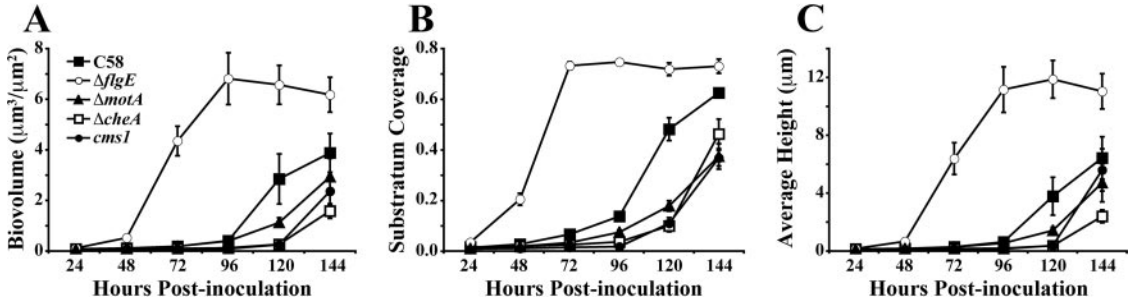

FIG. 5. Image analysis of flow cell biofilms. *auto*COMSTAT was used to determine the biovolume per substratum area (A), substratum coverage (B), and average overall height (C). Values are averages calculated for 15 image stacks collected from three channels (5 image stacks per channel) for each strain per time point. Error bars show SEM.

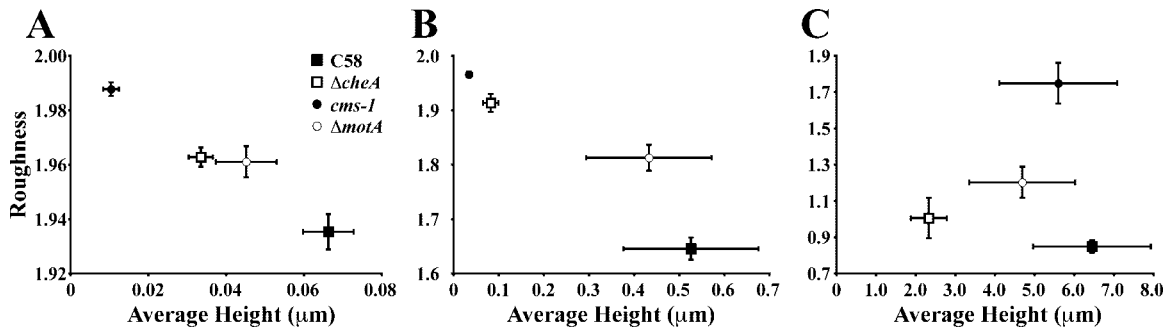

FIG. 6. Average height and roughness of flow cell biofilms at 48 (A), 96 (B), and 144 (C) hpi. Data are shown for C58 (closed squares), the Δ*cheA* mutant (open squares), the Δ*motA* mutant (open circles), and the *cms-1* mutant (closed circles). Note that the Δ*flgE* mutant was omitted from these comparisons because of the large differences in biofilm height. The coordinates (height, roughness) for the Δ*flgE* mutant were as follows: 0.563 μm, 1.532 at 48 hpi, 11.259 μm, 0.762 at 96 hpi, and 11.137 μm, 0.685 at 144 hpi. Error bars show SEM.

wild-type biofilms continued to accumulate for the duration of the experiment.

We also enumerated microcolonies, which we defined as adherent cell aggregates with a volume of at least 100 μm^3. The maximum number of microcolonies counted in the Δ*flgE* biofilms occurred at 48 hpi, corresponding to 20% substratum coverage (Fig. 5B; see Fig. S2 in the supplemental material). From 48 to 72 hpi, the number of microcolonies dropped fourfold, reflecting the increasing confluence of adherent growth. Wild-type biofilms reached a maximum number of microcolonies at 96 hpi, 2 days later than the Δ*flgE* mutant, but with similar amounts of colonized substratum (Fig. 5B; see Fig. S2 in the supplemental material). As the substratum coverage approached 60% at 144 hpi, the number of C58 microcolonies was approximately one per field of view, indicating nearly contiguous coverage of the substratum.

To further investigate the nature of the Δ*flgE* biofilm phenotype, we conducted a short-term flow cell experiment, making observations every 3 hours. For the first 9 hours, the Δ*flgE* mutant biovolume and substratum coverage values were slightly lower than those for the wild type, consistent with its attachment deficiency in static cultures (see Fig. S3 in the supplemental material). However, by 18 hpi, the Δ*flgE* mutant exceeded the wild type in both of these parameters. By 24 hpi, the amounts of Δ*flgE* biovolume and substratum coverage were approximately 1.5- to 2-fold higher than those of wild-type C58 (see Fig. S3 in the supplemental material).

The Δ*motA* mutant is severely compromised for biofilm formation in flow cells. Similar to the profound Δ*motA* mutant biofilm defect in static culture, the Δ*motA* mutant flow cell biofilms were dramatically reduced relative to those of the wild type. Early time points revealed limited numbers of attached cells and isolated microcolonies. Although large microcolonies had formed by 144 hpi, extensive areas of uncolonized substratum remained (Fig. 4C; see Fig. S1C in the supplemental material). The Δ*motA* mutant biofilms were debilitated in several of the numerical parameters analyzed, with approximately threefold reductions in biovolume, substratum coverage, and average height relative to those of the wild type by 120 hpi (Fig. 5). Even with these differences, the total biovolume and average height approached wild-type levels by 144 hpi (Fig. 5), and both strains had similar maximum heights of approximately 30 μm. However, biofilms formed by the Δ*motA* mutant had about 30% less substratum coverage than the wild type (Fig. 5). Consistent with this observation, the number of Δ*motA* microcolonies continued to increase through 144 hpi, revealing that the increases in total adherent biomass over time were constrained to specific sites on the surface (see Fig. S2 in the supplemental material).

Comparison of the average biofilm height and the roughness coefficient is a metric that has been proposed to represent biofilm complexity (16). The dimensionless roughness coefficient is a parameter that provides a measure of biofilm height variability. By this comparison, biofilms formed by the Δ*motA* mutant maintained an architecture significantly different from that of the wild type, with greater heterogeneity over the duration of the experiment (Fig. 6C).

Chemotaxis is required for normal biofilm formation in flow cells. The Δ*cheA* mutant manifested an aberrant biofilm phenotype in flow cells that was more pronounced than that in static culture biofilms. At early time points, very few cells were attached to the substratum. However by 144 hpi, the biofilms covered a substantial fraction of the available surface but were relatively homogeneous and short (Fig. 4D; see Fig. S1D in the supplemental material). The Δ*cheA* mutant biofilms also appeared to be less dense than those of the wild type or the nonmotile mutants (Fig. 4B and C; see Fig. S1D in the supplemental material). Qualitative observations were confirmed by *auto*COMSTAT analysis. The biomass and height of the Δ*cheA* mutant biofilms were roughly threefold lower than those of C58 biofilms by 144 hpi, with less overall substratum coverage (Fig. 5). Similar to the Δ*motA* biofilms, the number of microcolonies in biofilms of the Δ*cheA* mutant increased through 144 hpi (see Fig. S2 in the supplemental material). The comparison of average height to roughness reflected a distinct architecture for the Δ*cheA* biofilms throughout the experiment (Fig. 6).

Identification of a bypass suppressor of the Δ*cheA* motility agar phenotype. The motility agar phenotype of the Δ*cheA* mutant consistently exhibited an about 70% reduction in swim ring diameter relative to that of wild-type C58. Interestingly, after extended incubation, flares of diffuse growth began to emerge from the dense swim ring formed by the Δ*cheA* mutant (Fig. 7A). With time, these flares expanded to nearly cover the plate at a density similar to that of the wild type (data not shown). Bacteria isolated from the outer edges of these flares

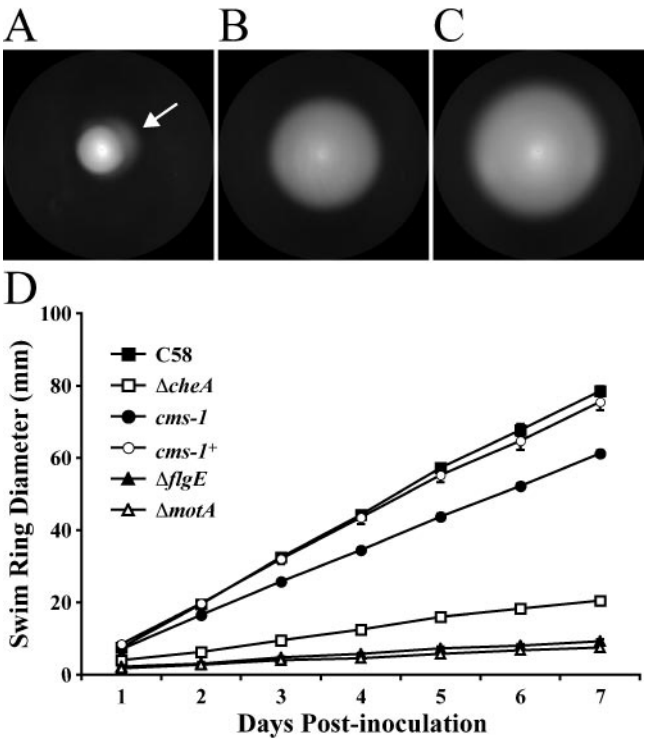

FIG. 7. Motility agar phenotype of the *cms-1* mutant. Swim plate images of the Δ*cheA* mutant showing suppressor flare (A), the *cms-1* mutant (B), and the *cms-1*/pPM109 mutant (C) are displayed. Image A was taken at 6 days postinoculation; images B and C were taken at 5 days postinoculation. The arrow shows the suppressor flare from the Δ*cheA* swim ring. (D) Quantified swim ring diameters of C58 (closed squares), the Δ*cheA* mutant (open squares), the Δ*flgE* mutant (closed triangles), the Δ*motA* mutant (open triangles), the *cms-1* mutant (closed circles), and the *cms-1*/pPM109 mutant (open circles). Values are the averages for four swim plates per strain. Error bars show SEM.

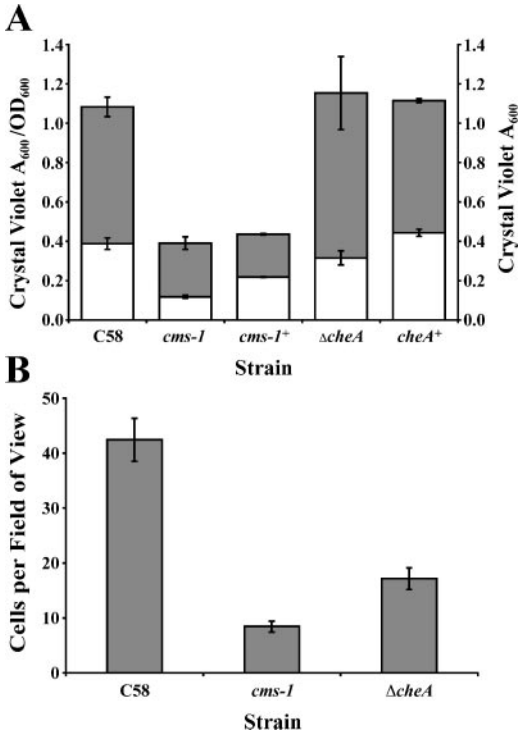

FIG. 8. Static biofilm formation and surface attachment by the *cms-1* mutant. (A) Quantification of DMSO-solubilized CV from PVC coverslip biofilms at 72 hpi. Biomass normalized for growth (A_{600}/OD_{600}; closed bars) and adherent biomass (CV A_{600}; open bars) are shown. +, strains carrying a wild-type copy of the deleted gene on pBBR1MCS-2. Error bars are SEM for three coverslips. (B) Static culture short-term binding assay. Total numbers of attached cells per field of view (~3.13×10^4 μm^2) are shown. Values are averages for 30 fields of view. Error bars show SEM.

exhibited a swim phenotype similar to that of the wild type (Fig. 7B). Quantitative analysis showed that swim ring diameters of a representative suppressor mutant, the *cms-1* mutant, were approximately 80% that of strain C58 (Fig. 7D). All putative suppressor isolates tested retained the *cheA* deletion. Additional chemotaxis mutants, including a mutant in which the entire chemotaxis operon was deleted (Atu0514 to Atu0522), also generated similar spontaneous suppressor mutations (data not shown). Microscopic examination revealed appreciable tumbling in the suppressor mutants, in contrast to the Δ*cheA* nontumbling phenotype. We designated this the Cms phenotype, for *C*he$^-$ *m*utation *s*uppressor. When a copy of *cheA* was expressed from a plasmid in the *cms-1* mutant, swim ring diameters were restored to normal (Fig. 7C and D).

***cms* mutants are impaired in biofilm formation in static culture and flow cells.** The *cms* mutants appeared to be nearly wild type in swimming behavior. However, in contrast to the wild type and their Δ*cheA* parent strain, the *cms* mutants exhibited profound biofilm formation deficiencies. In static culture coverslip biofilms, there was roughly 50% less attached *cms-1* biomass after 72 h of growth (Fig. 8A). Despite correcting the Cms swim plate phenotype to full wild-type levels (Fig. 7C and D), plasmid-based expression of wild-type *cheA* did not complement the biofilm defect (Fig. 8A). Similar to the case for the other motility and chemotaxis mutants, the *cms-1* mutant manifested a severe attachment deficiency in short-term binding assays (compare Fig. 8B to Fig. 3B).

Flow cell biofilms of the *cms-1* mutant were dramatically altered relative to those of the wild type (Fig. 4; see Fig. S1E in the supplemental material). Although similar to the Δ*cheA* mutant biofilms, several of the attributes of the *cms-1* biofilm were also distinct. *cms-1* biofilms attained an average height similar to that of the wild type by 144 hpi but were more structurally homogeneous and manifested significantly less surface coverage and overall biomass (Fig. 4E and 5). Late-stage *cms-1* biofilms were also less dense, with a roughness coefficient approximately twofold higher than that of the wild type, while both strains had similar average heights (Fig. 6C; also compare the orthogonal views in Fig. 4A and E).

DISCUSSION

In this study, we examined biofilm formation by defined *A. tumefaciens* C58 motility and chemotaxis mutants in both static and flow cell cultivation formats. We observed that the roles of motility and chemotaxis in biofilm formation differ significantly between these culture formats. The defined Fla$^-$ and Mot$^-$ mutants described here manifested severe deficiencies in at-

tachment and biofilm formation in static culture. Interestingly, the Δ*flgE* mutant biofilms grown in flow cells were greatly enhanced relative to those of the wild type, while the Δ*motA* biofilms remained severely debilitated. Chemotaxis mutants were more modestly affected in attachment and biofilm formation under static conditions but manifested a more severe defect in flow cells. Finally, a spontaneous suppressor mutation that restores tumbling to the straight-swimming Δ*cheA* mutant had a negative impact on biofilm formation in both static and flow cell cultures. The flow cell format allowed us to perform high-resolution comparisons of the wild type and mutant derivatives during the progression from initial attachment through mature biofilms (see Fig. S1 in the supplemental material).

Motility-driven surface interactions differentially influence biofilm formation between static and flowing environments. There have been few direct comparisons of biofilm formation by motile bacteria between static and flowing formats, particularly those that evaluate the roles for chemotaxis and motility. Under static culture conditions, a loss of motility should limit the ability of cells to interact with and subsequently attach to surfaces. Studies of *E. coli* Fla$^-$ and Mot$^-$ mutants suggested that motility per se is required for biofilm formation and that flagella do not function as inert adhesins (33). In contrast, Kirov et al. reported that the flagella of *Aeromonas* spp. function primarily as adhesins that promote attachment (20). If *A. tumefaciens* C58 flagella function strictly as adhesins, one would expect the phenotype of Δ*motA* mutation to be less pronounced than that of Δ*flgE* mutation. Our data clearly show that depending on the culture format, the Δ*motA* biofilm defect is equal to or more severe than that of the Δ*flgE* mutant, suggesting that active motility is required for attachment and biofilm maturation. Thus, flagella do not function as inert adhesins in C58. A modest yet consistent trend in our static biofilm assays suggests that the Δ*motA* mutation imparts a more severe defect than the Δ*flgE* mutation (data not shown). We therefore propose that the presence of unpowered flagella in the Δ*motA* mutant does in fact interfere with initial surface interactions and subsequent permanent attachment.

We expected biofilm phenotypes of the motility mutants to be less severe in flow cells because increased surface sampling, imparted by the flow of medium, would allow for more frequent attachment and subsequent biofilm formation. We were surprised, however, to find that the accumulation of adherent biomass was significantly accelerated for the C58 Δ*flgE* mutant. The adherent population was strikingly thicker than that of the wild type and had significant numbers of very tall and dense tower-like structures. Therefore, increasing the frequency of surface interactions relative to that under static conditions facilitates robust adherence and biofilm formation by the Δ*flgE* mutant.

In contrast, flow conditions did not ameliorate the Δ*motA* attachment defect, suggesting that paralyzed flagella may physically interfere with surface attachment. A recent report has shown that nonmotile *Listeria monocytogenes* mutants exhibit profound deficiencies in surface attachment (24). For aflagellate mutants, this attachment defect can be rescued by forcing cells to the surface via centrifugation, but this phenotype of mutants with paralyzed flagella is only partially rescued. These observations suggest that paralyzed flagella may block surface interactions and thereby limit attachment efficiency and biofilm formation. This is consistent with our findings that clearly indicate that for strain C58, unpowered flagella are not efficient adhesins in static or flowing environments and block productive surface interactions. Another possibility is that the flagella provide enhanced drag for the flowing medium to pull the cells away from the surface.

Lateral biofilm expansion without surface motility mechanisms. Biofilm expansion along surfaces involves a combination of multiple processes, including colonization from planktonic-phase cells, clonal growth of surface-associated cells, and in some systems, migration of previously attached cells via surface motility. In *P. aeruginosa*, twitching and swarming motilities promote lateral expansion and contribute to the overall architecture of the biofilm (21). Twitching and swarming have not been reported for C58 or other agrobacteria. The lateral accumulation of adherent biomass for C58 must therefore combine clonal growth of attached cells and new colonization by planktonic bacteria, the majority of which originate from the biofilm itself.

For nonflagellated C58 mutants in static cultures, we expected that the small fraction of cells colonizing the surface from the fluid phase would result in clonal microcolonies due to reduced lateral spreading, leading to a patchy biofilm. The punctate appearance of the Δ*flgE* coverslip biofilms is consistent with this prediction (data not shown). Flow cell biofilms of this mutant were comprised of strikingly tall microcolonies and rapidly formed dense surface populations (Fig. 4B and 5; see Fig. S3 in the supplemental material). This aberrant microcolony formation seems readily explained by clonal growth of adhered cells combined with limited dispersal. The overall adherent biomass for the Δ*flgE* mutant was, however, much greater than that of the wild type (Fig. 5A), suggesting additional roles for motility subsequent to initial colonization and microcolony formation.

For many motile bacteria, there is a period of reversible attachment during which cells can detach and sample additional surfaces (43). It is likely that in the absence of swimming motility, Δ*flgE* mutant cells at the surface frequently transition to irreversible attachment because there is no mechanism by which the cells can actively detach. The frequency at which bacteria detach from surfaces will have a significant impact on the growth and architecture of the biofilm. In the wild type, the rate of biomass increase on the surface is contingent upon active emigration of motile cells into the planktonic phase. In contrast, Δ*flgE* cells cannot actively detach, thus constraining their escape from the surface relative to that of the wild type. This effect would grow to be more pronounced as the attached biomass accumulates, thereby increasing the total number of cells near the surface. Examination of early stages of biofilm formation revealed that the marked increase in the Δ*flgE* biofilm occurred several hours after the initial attachment during the maturation phase (see Fig. S3 in the supplemental material). These nonmotile bacteria are limited to passive surface interactions and likely colonize proximal to their site of origin, leading to rapid accumulation of dense biofilms.

Chemotaxis influences biofilm structure under flow conditions. The role of chemotaxis in bacterial biofilm formation is unclear, with different reports concluding that chemotaxis is either required or dispensable, depending on the model sys-

tem. For example, Pratt and Kolter concluded that chemotaxis is fully dispensable for biofilm formation in *E. coli* (33). In contrast, *Aeromonas* sp. chemotaxis mutants have been shown to have a severe biofilm defect in static culture (20). Collectively, these observations indicate that there are species-specific differences in the requirement for chemotaxis during biofilm formation.

While the static culture biofilm deficiency manifested by the Δ*cheA* mutant appears to be mild when corrected for culture growth, short-term binding assays showed that this mutant is in fact significantly impaired for surface attachment (Fig. 3B). This defect is largely independent of growth because the short time scale of these experiments does not allow extensive cell division to occur. Therefore, the Δ*cheA* mutant attachment and biofilm phenotypes strongly suggest that there is a role for chemotaxis, and therefore regulated motility, in surface sampling, attachment, and subsequent biofilm formation. Flow cell biofilms of the Δ*cheA* mutant were consistently less confluent and more structurally homogeneous than those of the wild type (Fig. 5). The decreased density of mature Δ*cheA* biofilms (Fig. 4D) may reflect reduced attachment efficiency as well as a role for chemotaxis in determining the cellular organization within the biofilm and, ultimately, its architecture. Although this phenotype could also be influenced by reduced growth of the Δ*cheA* mutant, the unique structural attributes (Fig. 4 and 6) of this biofilm strongly suggest more specific roles for chemotaxis in biofilm formation.

A chemotaxis mutant suppressor reveals the importance of appropriate flagellar control in biofilm formation. During the analysis of our Δ*cheA* mutant, we isolated the *cms* suppressors of the Che$^-$ swim defect and subsequently found these mutants to be profoundly debilitated for biofilm formation. The observed restoration of tumbling in the suppressor mutants was not due to a true reversal of the chemotaxis phenotype, as demonstrated by the normal swim ring diameter of a *cms-1* mutant expressing a plasmid-borne *cheA* gene (Fig. 7). Suppression was also observed in other Che$^-$ mutants, including one with a clean deletion of the entire *che* operon, and therefore it is likely that the swimming phenotype of the suppressor functions independently of the chemotaxis system. The Cms phenotype bears facile similarity to a swim plate phenotype described as pseudotaxis, which is correlated with increased tumbling in an *E. coli* mutant containing a deletion of the entire *che* operon (44). Several *E. coli* and *Salmonella enterica* serovar Typhimurium pseudotaxis mutations have been mapped to the flagellar switch gene *fliM* (38). These FliM mutations increase the basal frequency of rotational switching for the flagella, resulting in a larger swim ring diameter on motility plates (38, 44). We have not identified any mutations in *fliM* (Atu0561) or several other C58 candidate genes which could influence tumbling frequency (data not shown), although this does not rule out the possibility that the *cms* mutants are pseudotactic.

The *cms-1* mutant is severely deficient in attachment and subsequent biofilm formation under static conditions. This biofilm phenotype was not rescued by complementation with *cheA*, suggesting that the *cms-1* defect is independent of chemotaxis. It is plausible that the restored yet aberrant tumbling exhibited by the *cms-1* mutant interferes with productive surface interactions. Although it is formally possible that this mutation leads to an additional defect unrelated to motility, this seems unlikely given the overall importance of this process in C58 biofilm formation.

In contrast to static culture, biofilms of the *cms-1* mutant and its Δ*cheA* parent were strikingly similar in flow cells, though notable differences remained. Biofilms of the *cms-1* mutant had greater average heights and were even less densely packed with cells than the Δ*cheA* biofilms (Fig. 4 and 5). The biofilm deficiencies manifested by the *cms-1* mutant, in either a flowing or static environment, indicate that the renewed tumbling exhibited by this mutant does not promote productive surface interactions. The control of flagellar rotation is likely to be critical for initial attachment and the subsequent transition from a planktonic to a sessile state. Identification of the mutation(s) underlying the Cms suppression phenotype should provide insights into how *A. tumefaciens* coordinates control of flagellar activity during the early stages of biofilm formation.

Motility and chemotaxis during the transition to sessile growth. One reasonable model for the role of motility and chemotaxis in biofilm formation by strain C58 is that the transition from initial to permanent attachment requires regulation of flagellar rotation. In static culture, flagella serve to promote surface interactions by propelling cells to the surface. The efficiency and frequency of surface sampling may be influenced through chemotactic processes. During the sampling period, the flagella are still able to rotate, allowing cells to return to the planktonic phase. Once the transition to a sessile growth state has been made, motility is no longer required. As the biofilm matures, other signals, such as chemotactic cues, may stimulate renewed motility. Bacteria released into the planktonic phase have the potential to colonize new sites and promote lateral expansion of the biofilm. Our findings show that both motility and chemotaxis contribute to biofilm formation and demonstrate the significant influence of the prevailing environment on their respective functions. *A. tumefaciens* C58 differs from other biofilm model systems, such as *P. aeruginosa*, in its lack of surface motility. This allows analysis of the effects of swimming motility without the confounding processes of twitching or swarming.

ACKNOWLEDGMENTS

We acknowledge Michael Hibbing, Yves Brun, Dan Kearns, Tom Platt, and Cécile Berne for helpful discussions. Cheríe Blair provided valuable technical support.

This project was supported by National Institutes of Health grant GM080546 and through a grant from the Indiana University META-Cyt program, funded in part by a major endowment from the Lilly Foundation.

REFERENCES

1. **Adler, J.** 1966. Chemotaxis in bacteria. Science **153:**708–716.
2. **An, D., T. Danhorn, C. Fuqua, and M. R. Parsek.** 2006. Quorum sensing and motility mediate interactions between *Pseudomonas aeruginosa* and *Agrobacterium tumefaciens* in biofilm cocultures. Proc. Natl. Acad. Sci. USA **103:** 3828–3833.
3. **Armitage, J. P., and R. Schmitt.** 1997. Bacterial chemotaxis: *Rhodobacter sphaeroides* and *Sinorhizobium meliloti*--variations on a theme? Microbiology **143:**3671–3682.
4. **Berg, H. C.** 2003. The rotary motor of bacterial flagella. Annu. Rev. Biochem. **72:**19–54.
5. **Burr, T. J., B. H. Katz, and A. L. Bishop.** 1987. Populations of *Agrobacterium* in vineyard and nonvineyard soils and grape roots in vineyards and nurseries. Plant Dis. **71:**617–620.
6. **Chesnokova, O., J. B. Coutinho, I. H. Khan, M. S. Mikhail, and C. I. Kado.** 1997. Characterization of flagella genes of *Agrobacterium tumefaciens*, and the effect of a bald strain on virulence. Mol. Microbiol. **23:**579–590.

7. **Christensen, B. B., C. Sternberg, J. B. Andersen, R. J. J. Palmer, A. T. Nielsen, M. Givskov, and S. Molin.** 1999. Molecular tools for study of biofilm physiology. Methods Enzymol. **310:**20–42.
8. **Christie, P. J.** 2001. Type IV secretion: intercellular transfer of macromolecules by systems ancestrally related to conjugation machines. Mol. Microbiol. **40:**294–305.
9. **Cormack, B. P., R. H. Valdivia, and S. Falkow.** 1996. FACS-optimized mutants of the green fluorescent protein (GFP). Gene **173:**33–38.
10. **Danhorn, T., M. Hentzer, M. Givskov, M. Parsek, and C. Fuqua.** 2004. Phosphorus limitation enhances biofilm formation of the plant pathogen *Agrobacterium tumefaciens* through the PhoR-PhoB regulatory system. J. Bacteriol. **186:**4492–4501.
11. **Escobar, M. A., and A. M. Dandekar.** 2003. *Agrobacterium tumefaciens* as an agent of disease. Trends Plant Sci. **8:**380–386.
12. **Fuqua, W. C., and S. C. Winans.** 1994. A LuxR-LuxI-type regulatory system activates *Agrobacterium* Ti plasmid conjugal transfer in the presence of a plant tumor metabolite. J. Bacteriol. **176:**2796–2806.
13. **Galibert, F., T. M. Finan, S. R. Long, A. Puhler, P. Abola, F. Ampe, F. Barloy-Hubler, M. J. Barnett, A. Becker, P. Boistard, G. Bothe, M. Boutry, L. Bowser, J. Buhrmester, E. Cadieu, D. Capela, P. Chain, A. Cowie, R. W. Davis, S. Dreano, N. A. Federspiel, R. F. Fisher, S. Gloux, T. Godrie, A. Goffeau, B. Golding, J. Gouzy, M. Gurjal, I. Hernandez-Lucas, A. Hong, L. Huizar, R. W. Hyman, T. Jones, D. Kahn, M. L. Kahn, S. Kalman, D. H. Keating, E. Kiss, C. Komp, V. Lelaure, D. Masuy, C. Palm, M. C. Peck, T. M. Pohl, D. Portetelle, B. Purnelle, U. Ramsperger, R. Surzycki, P. Thebault, M. Vandenbol, F. J. Vorholter, S. Weidner, D. H. Wells, K. Wong, K. C. Yeh, and J. Batut.** 2001. The composite genome of the legume symbiont *Sinorhizobium meliloti*. Science **293:**668–672.
14. **Gelvin, S. B.** 2003. *Agrobacterium*-mediated plant transformation: the biology behind the "gene-jockeying" tool. Microbiol. Mol. Biol. Rev. **67:**16–37.
15. **Goodner, B., G. Hinkle, S. Gattung, N. Miller, M. Blanchard, B. Qurollo, B. S. Goldman, Y. Cao, M. Askenazi, C. Halling, L. Mullin, K. Houmiel, J. Gordon, M. Vaudin, O. Iartchouk, A. Epp, F. Liu, C. Wollam, M. Allinger, D. Doughty, C. Scott, C. Lappas, B. Markelz, C. Flanagan, C. Crowell, J. Gurson, C. Lomo, C. Sear, G. Strub, C. Cielo, and S. Slater.** 2001. Genome sequence of the plant pathogen and biotechnology agent *Agrobacterium tumefaciens* C58. Science **294:**2323–2328.
16. **Heydorn, A., A. Toftgaard Nielsen, M. Hentzer, C. Sternberg, M. Givskov, B. Kjaer Ersbøll, and S. Molin.** 2000. Quantification of biofilm structures by the novel computer program COMSTAT. Microbiology **146:**2395–2407.
17. **Kado, C. I.** 1992. Plant pathogenic bacteria, p. 659–674. *In* A. I. Balows, H. G. Truper, M. Dworkin, W. Harder, and K.-H. Schleifer (ed.), The prokaryotes, 2nd ed., vol. 1. Springer-Verlag, New York, NY.
18. **Kaniga, K., I. Delor, and G. R. Cornelis.** 1991. A wide-host-range suicide vector for improving reverse genetics in gram-negative bacteria: inactivation of the *blaA* gene of *Yersinia enterocolitica*. Gene **109:**137–141.
19. **Kim, H., and S. K. Farrand.** 1998. Opine catabolic loci from *Agrobacterium* plasmids confer chemotaxis to their cognate substrates. Mol. Plant-Microbe Interact. **11:**131–143.
20. **Kirov, S. M., M. Castrisios, and J. G. Shaw.** 2004. *Aeromonas* flagella (polar and lateral) are enterocyte adhesins that contribute to biofilm formation on surfaces. Infect. Immun. **72:**1939–1945.
21. **Klausen, M., A. Heydorn, P. Ragas, L. Lambertsen, A. Aaes-Jørgensen, S. Molin, and T. Tolker-Nielsen.** 2003. Biofilm formation by *Pseudomonas aeruginosa* wild type, flagella and type IV pili mutants. Mol. Microbiol. **48:**1511–1524.
22. **Kovach, M. E., P. H. Elzer, D. S. Hill, G. T. Robertson, M. A. Farris, R. M. I. Roop, and K. M. Peterson.** 1995. Four new derivatives of the broad-host-range cloning vector pBBR1MCS, carrying different antibiotic resistance cassettes. Gene **166:**175–176.
23. **Labbate, M., S. Y. Queck, K. S. Koh, S. A. Rice, M. Givskov, and S. Kjelleberg.** 2004. Quorum sensing-controlled biofilm development in *Serratia liquefaciens* MG1. J. Bacteriol. **186:**692–698.
24. **Lemon, K. P., D. E. Higgins, and R. Kolter.** 2007. Flagellar motility is critical for *Listeria monocytogenes* biofilm formation. J. Bacteriol. **189:**4418–4424.
25. **Mattick, J. S.** 2002. Type IV pili and twitching motility. Annu. Rev. Microbiol. **56:**289–314.
26. **Mayfield, C. I., and W. E. Inniss.** 1977. A rapid, simple method for staining bacterial flagella. Can. J. Microbiol. **23:**1311–1313.
27. **McBride, M. J.** 2001. Bacterial gliding motility: multiple mechanisms for cell movement over surfaces. Annu. Rev. Microbiol. **55:**49–75.
28. **Mersereau, M., G. J. Pazour, and A. Das.** 1990. Efficient transformation of *Agrobacterium tumefaciens* by electroporation. Gene **90:**149–151.
29. **Miller, J. F., J. J. Mekalanos, and S. Falkow.** 1989. Coordinate regulation and sensory transduction in the control of bacterial virulence. Science **243:**916–922.
30. **Miller, V. L., and J. J. Mekalanos.** 1988. A novel suicide vector and its use in construction of insertion mutations: osmoregulation of outer membrane proteins and virulence determinants in *Vibrio cholerae*. J. Bacteriol. **170:**2575–2583.
31. **Moorthy, S., and P. I. Watnick.** 2004. Genetic evidence that the Vibrio cholerae monolayer is a distinct stage in biofilm development. Mol. Microbiol. **52:**573–587.
32. **O'Toole, G. A., and R. Kolter.** 1998. Flagellar and twitching motility are necessary for *Pseudomonas aeruginosa* biofilm development. Mol. Microbiol. **30:**295–304.
33. **Pratt, L. A., and R. Kolter.** 1998. Genetic analysis of *Escherichia coli* biofilm formation: roles of flagella, motility, chemotaxis and type I pili. Mol. Microbiol. **30:**285–293.
34. **Ramey, B. E., A. G. Matthysse, and C. Fuqua.** 2004. The FNR-type transcriptional regulator SinR controls maturation of *Agrobacterium tumefaciens* biofilms. Mol. Microbiol. **52:**1495–1511.
35. **Sambrook, J., E. Fritsch, and T. Maniatis.** 1989. Molecular cloning: a laboratory manual. Cold Spring Harbor Laboratory Press, Cold Spring Harbor, NY.
36. **Schmitt, R.** 2002. Sinorhizobial chemotaxis: a departure from the enterobacterial paradigm. Microbiology **148:**627–631.
37. **Shaw, C. H., A. M. Ashby, A. Brown, C. Royal, G. J. Loake, and C. H. Shaw.** 1988. VirA and VirG are the Ti-plasmid functions required for chemotaxis of *Agrobacterium tumefaciens* towards acetosyringone. Mol. Microbiol. **2:**413–417.
38. **Sockett, H., S. Yamaguchi, M. Kihara, V. M. Irikura, and R. M. Macnab.** 1992. Molecular analysis of the flagellar switch protein FliM of *Salmonella typhimurium*. J. Bacteriol. **174:**793–806.
39. **Tempé, J., A. Petit, M. Holsters, M. Van Montagu, and J. Schell.** 1977. Thermosensitive step associated with transfer of the Ti plasmid during conjugation: possible relation to transformation in crown gall. Proc. Natl. Acad. Sci. USA **74:**2848–2849.
40. **Wadhams, G. H., and J. P. Armitage.** 2004. Making sense of it all: bacterial chemotaxis. Nat. Rev. Mol. Cell Biol. **5:**1024–1037.
41. **Warrens, A. N., M. D. Jones, and R. I. Lechler.** 1997. Splicing by overlap extension by PCR using asymmetric amplification: an improved technique for the generation of hybrid proteins of immunological interest. Gene **186:**29–35.
42. **Watson, B., T. C. Currier, M. P. Gordon, M. D. Chilton, and E. W. Nester.** 1975. Plasmid required for virulence of *Agrobacterium tumefaciens*. J. Bacteriol. **123:**255–264.
43. **Webb, J. S., M. Givskov, and S. Kjelleberg.** 2003. Bacterial biofilms: prokaryotic adventures in multicellularity. Curr. Opin. Microbiol. **6:**578–585.
44. **Wolfe, A. J., and H. C. Berg.** 1989. Migration of bacteria in semisolid agar. Proc. Natl. Acad. Sci. USA **86:**6973–6977.
45. **Wood, D. W., J. C. Setulab, R. Kaul, D. E. Monks, J. P. Kitajima, V. K. Okura, Y. Zhou, L. Chen, G. E. Wood, N. F. J. Almeida, L. Woo, Y. Chen, I. T. Paulsen, J. A. Eisen, P. D. Karp, D. S. Dovee, P. Chapman, J. Clendenning, G. Deatherage, W. Gillet, C. Grant, T. Kutyavin, R. Levy, M.-J. Li., E. McClellund, A. Palmieri, C. Raymond, G. Rouse, C. Saenphimmachak, Z. Wu, P. Romero, D. Gordon, S. Zhang, H. Yoo, Y. Tao, P. Biddle, M. Jung, W. Krespan, M. Perry, B. Gordon-Kamm, L. Liao, S. Kim, C. Hendrick, Z.-Y. Zhao, M. Dolan, F. Chumley, S. V. Tingey, J.-F. Tomb, M. Gordon, M. V. Olson, and E. W. Nester.** 2001. The genome of the natural genetic engineer *Agrobacterium tumefaciens* C58. Science **294:**2317–2323.
46. **Wright, E. L., W. J. Deakin, and C. H. Shaw.** 1998. A chemotaxis cluster from *Agrobacterium tumefaciens*. Gene **220:**83–89.